J. Fluid Mech. (1985), *vol.* 159, *pp.* 259–287
Printed in Great Britain

The stability of flows in channels with small wall curvature

By G. A. GEORGIOU

Topexpress Ltd, Scientific and Computer Consultants,
13/14 Round Church St, Cambridge CB5 8AD

AND P. M. EAGLES

Department of Mathematics, The City University, London EC1

(Received 21 November 1983 and in revised form 23 April 1985)

The 'stability' of flows in symmetric curved-walled channels is investigated by essentially combining Fraenkel's 'small' wall-curvature theory with the multiple-scaling (or WKB) method. The basic flow is characterized by the steady-state stream function Ω, which varies 'slowly' in the streamwise direction. An asymptotic scheme is posed for Ω in such a way that at lowest order Ω represents a class of Jeffery–Hamel solutions. An infinitesimal disturbance is superimposed on the basic flow through a time-dependent stream function Φ, and the resulting linearized disturbance equation suggests that fixed-frequency disturbances with 'slowly' varying wavenumber are appropriate. The asymptotic scheme for Φ yields the Orr–Sommerfeld equation at lowest order. Two classes of channels are considered. In the first class the curvature is constant in sign, and under certain conditions they reduce to symmetric divergent straight-walled channels. In the second class of channels the curvature varies in sign, and these may be more suitable for experimentation. A spatially dependent growth rate of the disturbance relative to the basic flow is defined; this forms the basis of the 'stability' analysis. Critical Reynolds numbers are deduced, below which the disturbance decays as it travels downstream, and above which the disturbance grows for a limited range in the streamwise direction. For the first class of channels the 'stability' analysis is carried out locally, and the dependence of the critical Reynolds numbers on curvature and higher-order terms is investigated. For the second class of channels the 'stability' analysis is carried out at various positions downstream, and an overall minimum critical Reynolds number is predicted for a range of channels and flows.

1. Introduction

During recent years there has been considerable interest in the 'stability' of slightly non-parallel flows considered in the light of the so-called WKB method. In this method the basic flow (for example the Blasius boundary layer or the flow between divergent planes) is expressed in such a way that it depends upon a 'slow' streamwise variable $X = \epsilon x$, where ϵ is a small parameter. It is then found that a time-dependent linear disturbance satisfies a differential equation whose coefficients depend on X. Thus fixed-frequency disturbances of the form

$$\chi = \exp(\mathrm{i}S - \mathrm{i}\omega t)\, g(X, y; \epsilon)$$

are appropriate. Here the frequency w is real, y is a cross-stream variable and

$$\frac{\mathrm{d}S}{\mathrm{d}x} = Q(X)$$

is assumed, so that the spatial growth rate to first order is $-Q_i$, where Q_i is the imaginary part of Q. Upon expanding the base flow and $g(X, y; \epsilon)$ in powers of ϵ, it is found that the growth rate in the streamwise direction is modified from that obtained by quasiparallel theory, thus leading to different values of the critical Reynolds number.

This type of technique has been used, for example, by Bouthier (1972, 1973), Gaster (1974) and Smith (1979) for the boundary layer, by Drazin (1974) for a model problem, by Eagles & Weissman (1975) for flow in a wedge, by Eagles & Smith (1980) for flow in a channel whose walls have equations $y = H(X)$ and by Zollars & Krantz (1980) for film flow down a right-circular cone.

The present investigation applies the technique to flow in symmetric channels with 'small' wall curvature within the framework of Fraenkel's (1962, 1963) steady-state theory. In §2 the Navier–Stokes equations are written for an incompressible viscous fluid, and are expressed in terms of Fraenkel's coordinate system (ξ, η), where ξ is the streamwise variable and η is the cross-stream variable. We consider the channels to be of unit depth, and to represent some section of much larger channels which are unrestricted in the direction normal to the (ξ, η)-plane. In this way the flow properties are assumed to be independent of this direction, and the problem is reduced to a two-dimensional one.

Two classes of symmetric curved-walled channels are defined using Fraenkel's 'slowly' varying complex function $\alpha(\tau)$, where $\tau = \sigma + \mathrm{i}\epsilon\eta$ and $\sigma = \epsilon\xi$ are 'slow' variables. It can be shown (Fraenkel 1963) that $|\alpha(\sigma)|$ is approximately the local semidivergence of the channel walls. Certain restrictions are necessarily imposed on $\alpha(\tau)$. One restriction ensures that the local wall curvature is 'small'. Fraenkel (1963) characterizes the 'small' curvature of the channel walls by the property

$$|\text{local wall curvature} \times \text{local channel half-width}| \leqslant \epsilon.$$

Other restrictions ensure that the base flow is described by an asymptotic expansion whose first term satisfies the nonlinear ordinary differential equation (22), while higher-order terms are required to take account of curvature. This is achieved by choosing $\alpha(\tau)$ and the Reynolds number R to satisfy

$$R\alpha = O(1) \quad \text{as } \epsilon \to 0,$$

$$R\epsilon = \delta \to 0 \quad \text{as } \epsilon \to 0.$$

The choice of $R = v/\epsilon^{\frac{1}{2}}$ and $\alpha(\tau) = \epsilon^{\frac{1}{2}}\alpha'(\tau)$, where $\alpha'(\tau)$ is some function not containing the small parameter ϵ explicitly, satisfy the conditions. These points are discussed in §3.

For general R and $\epsilon^{\frac{1}{2}}$ there are infinitely many mathematical solutions to (22) (Rosenhead 1940). Fraenkel (1962) shows that for these solutions to be unique and to correspond to the simpler types, that is, with symmetric velocity profiles (about $\eta = 0$) and at most one region of reversed flow near the walls, then the range of v is restricted. The range considered here ($0 \leqslant v \leqslant 5$) is within the range defined by Fraenkel and includes the case when reversed flow is first achieved ($v \approx 4.7$).

It is important to note that, if the above relationship between R and $\epsilon^{\frac{1}{2}}$ is enforced in the asymptotic development of the linear disturbance problem (26), then this will lead to a singular perturbation problem. In order to avoid this the relationship is relaxed, but is recalled in the final analysis of the results. The details of this approach

are discussed in §5. The asymptotic development now yields the classic Orr–Sommerfeld problem at lowest order, where the intrinsic frequency β_I and the complex wavenumber k are functions of a 'slow' variable.

The first choice of $\alpha(\tau)$, (12), defines channels whose curvature is constant in sign (figure 1). Under a certain asymptotic limit (14*b*) these channels reduce to the straight-walled channels studied by Eagles & Weissman (1975). One aim of this investigation is to use this property, not merely to check their results by an independent method, but also to consider the effects of curvature and higher-order terms on both the steady-state (16) and linear-disturbance (26) problems.

The results for the steady-state problem, which are presented in §4, show that, while higher-order terms compound any reversed flow near the walls (figure 2), curvature effects oppose and dominate higher-order effects (figure 3). The effects of including higher-order terms on the local 'stability' of the disturbance are small, but they do produce an interesting feature (figure 9). On the other hand the effects of curvature are more pronounced and are not negligible when calculating the critical Reynolds number R_c (table 3, figure 13).

The second choice of $\alpha(\tau)$, (56), defines channels whose curvature varies in sign (figure 17). The aim here is to investigate the local 'stability' of flows at different positions in the streamwise direction, and in doing so establish an overall criterion for 'stability' in the channel. These channels satisfy the conditions required by Fraenkel (1963), that is, $\alpha(\tau) \to 0$ as $\sigma \to \pm\infty$ and $\alpha(\tau)$ is real on $\eta = 0$. The results are presented in §8. The most 'unstable' regions in the channel are shown to be downstream of the position where the angle of divergence reaches its maximum value. A particular case for experimentation is illustrated.

Shen's (1961) arguments for measuring the temporal growth rate of the disturbance relative to the unsteady base flow are adapted for non-parallel basic flows (§6). A disturbance function $\hat{E} = E/E_0$ is used to define the spatial growth rate $\mathrm{GR}_\xi(\hat{E})$ of the disturbance. We define E to be the mean kinetic-energy density of the disturbance (averaged over one period π/β) and E_0 to be the kinetic-energy density of the basic flow. This definition implies that if $\mathrm{GR}_\xi(\hat{E}) < 0$ the disturbance is decreasing relatively at some value of σ, and we say the flow is 'locally stable'. Similarly, if $\mathrm{GR}_\xi(\hat{E}) > 0$ the disturbance is increasing relatively at some value of σ, and we say the flow is 'locally unstable'. The terms 'stable' and 'unstable' are used in this special sense. The interpretation of 'unstable', however, is not straightforward, since the flow may pass through a region of growth ('locally unstable') followed by a region of decay ('locally stable'). For the channels considered here it is found that all disturbances that grow eventually decay far enough downstream. It may appear that the flow is stable in a global sense, since the disturbance does not grow for all $\sigma > \sigma_0$, no matter how large $\mathrm{GR}_\xi(\hat{E})$ is. Nevertheless, the mechanism is present for transferring energy from the basic flow to the disturbance, and for disturbances where $\mathrm{GR}_\xi(\hat{E})$ is larger than some threshold value the flow in practice may be unstable.

2. The governing equations

Consider the Navier–Stokes equations in two dimensions for an incompressible viscous fluid. We can express these equations, using general orthogonal coordinates (a_1, a_2), in terms of the dimensional stream function $\hat{\Psi}$ (Goldstein 1938). With the usual denotation for ∇, we write

$$\frac{\partial}{\partial T}(\nabla^2\hat{\Psi}) + \frac{1}{h_1 h_2}\left[\frac{\partial\hat{\Psi}}{\partial a_2}\frac{\partial}{\partial a_1}(\nabla^2\hat{\Psi}) - \frac{\partial\hat{\Psi}}{\partial a_1}\frac{\partial}{\partial a_2}(\nabla^2\hat{\Psi})\right] = \nu\nabla^4\hat{\Psi}. \tag{1}$$

The cordinate system to be used follows Fraenkel's (1963) notation, and is recalled here for reference. Fraenkel defines a conformal transformation $Z = Z(\zeta)$ by

$$\frac{\mathrm{d}Z}{\mathrm{d}\zeta} = H(\xi, \eta) \exp(\mathrm{i}\vartheta(\xi, \eta)), \tag{2}$$

with $Z = X + \mathrm{i}Y$ ((X, Y) denote the dimensional Cartesian coordinates) and $\zeta = \xi + \mathrm{i}\eta$ ((ξ, η) denote the non-dimensional orthogonal coordinates). Here H is a dimensional scaling factor, and it can be shown that $2H$ is approximately the width of the channel corresponding to ξ = constant (Fraenkel 1962, 1963). The parameter ϑ is the angle between the elements of the two systems. Fraenkel goes on to define $\kappa(\xi, \eta)$ and $\lambda(\xi, \eta)$ by

$$\frac{\mathrm{d}}{\mathrm{d}\zeta}\left(\ln\frac{\mathrm{d}Z}{\mathrm{d}\zeta}\right) = \kappa(\xi, \eta) - \mathrm{i}\lambda(\xi, \eta) = \mu(\zeta), \tag{3}$$

and shows using (2) and (3) that κ/H and λ/H represent the curvatures in the Z-plane of the coordinate lines corresponding to ξ = constant and η = constant respectively. The curvatures of the channel walls are defined at $\eta = \pm 1$.

The form of (1) can be transformed in terms of Fraenkel's general orthogonal coordinates (ξ, η) with $h_1 = h_2 = H$, $a_1 = \xi$ and $a_2 = \eta$. The non-dimensional equation is found by setting

$$\hat{\Psi} = M\Psi, \quad H = bh, \quad T = \frac{b^2 t}{M}, \tag{4}$$

where M is defined to be half the volumetric flow rate per unit thickness and $2b$ is approximately the throat width of the channel under consideration at $\xi = 0$. Thus (1) may be written as

$$\left\{\frac{1}{R}\left(\mathrm{D}^2 - 4\left(\kappa\frac{\partial}{\partial\xi} + \lambda\frac{\partial}{\partial\eta}\right) + 4(\kappa^2 + \lambda^2)\right) - h^2\frac{\partial}{\partial t} - \left(\frac{\partial\Psi}{\partial\eta}\frac{\partial}{\partial\xi} - \frac{\partial\Psi}{\partial\xi}\frac{\partial}{\partial\eta} - 2\kappa\frac{\partial\Psi}{\partial\eta} + 2\lambda\frac{\partial\Psi}{\partial\xi}\right)\right\}\mathrm{D}^2\Psi = 0, \tag{5}$$

where $\mathrm{D}^2 \equiv \partial^2/\partial\xi^2 + \partial^2/\partial\eta^2$, and the boundary conditions are given by

$$\Psi = \pm 1 \quad \text{at } \eta = \pm 1, \tag{6a}$$

$$\frac{\partial\Psi}{\partial\eta} = 0 \quad \text{at } \eta = \pm 1, \tag{6b}$$

where (6a) defines M and (6b) is the no-slip condition at the walls of the channel. The Reynolds number R is defined by

$$R = \frac{M}{\nu}, \tag{7}$$

so that it does not vary from station to station in the channel (Rosenhead 1940); ν is the kinematic viscosity.

3. A symmetric curved-walled channel

The non-dimensional forms of (2) and (3) are found using (4) and defining $Z = bz$. Fraenkel (1963) shows that when the complex function $\mu(\zeta)$ in (3) is chosen to be a real constant α then α is exactly the semidivergence of the channel walls. For a more

general case Fraenkel introduces a small constant parameter ϵ such that

$$\epsilon\zeta = \tau, \quad \epsilon\xi = \sigma, \quad \tau = \sigma + i\epsilon\eta, \tag{8}$$

and posing

$$\mu(\zeta) = \alpha(\tau); \tag{9}$$

he goes on to show that the local semidivergence angle of the channel wall at $\eta = +1$, $\vartheta(\xi, 1)$, is approximately given by $\alpha(\sigma)$, and at $\eta = -1$, $\vartheta(\xi, -1)$, is approximately $-\alpha(\sigma)$. In this sense we may regard the slowly varying complex function $\alpha(\tau)$ as being like the local semidivergence of the channel walls upon setting $\eta = \pm 1$. However, the choice of $\alpha(\tau)$ depends on necessary conditions imposed on other parameters, namely R and ϵ.

Briefly, Fraenkel's asymptotic development of the solution to (5) (in steady-state form) is based on

$$\epsilon \to 0 \quad \text{with } \sigma, \eta \text{ fixed.} \tag{10}$$

Fraenkel poses and justifies an asymptotic expansion in ascending powers of ϵ. An alternative method, which he uses for computational purposes, is based on a double series expansion in ascending powers of $1/R^2$ and δ, where $\delta = R\epsilon$. In each case the following conditions had to be satisfied:

$$R\alpha = O(1) \quad \text{as } \epsilon \to 0, \tag{11a}$$

$$R\epsilon = \delta \to 0 \quad \text{as } \epsilon \to 0. \tag{11b}$$

In the first channel α is chosen to be

$$\alpha(\tau) = l\epsilon^{\frac{1}{2}} + \epsilon^{\frac{1}{2}} m\tau, \tag{12}$$

where m is a curvature parameter and l is a parameter whose significance is discussed in §8. If $m > 0$ the physical curvature of the channel wall corresponding to $\eta = +1$ is always positive, while for $m < 0$ the equivalent physical curvature is negative. If $m = 0$ the channel is straight-walled with total angle of divergence $2l\epsilon^{\frac{1}{2}}$. The choice of $\alpha(\tau)$ above and

$$R = \frac{v}{\epsilon^{\frac{1}{2}}} \tag{13a}$$

ensure that (11 *a*, *b*) are satisfied. The interpretation of v will become apparent in §4.

Under the asymptotic limit given by (10) and this choice of $\alpha(\tau)$, problems of unboundedness are encountered in the time-dependent analysis. In particular, the expression for h, the non-dimensional scaling factor, is found to be

$$h = C \exp\left[\frac{l\sigma}{\epsilon^{\frac{1}{2}}} + \frac{m\sigma^2}{2\epsilon^{\frac{1}{2}}} - \frac{m\epsilon^{\frac{3}{2}}\eta^2}{2}\right], \tag{13b}$$

upon substituting $\alpha(\tau)$ into (3) and comparing the integral with (2). This shows that $h \to \infty$ asymptotically as $\epsilon \to 0$. One way of overcoming this problem is to introduce a new slow variable. It is not necessary for the steady-state problem, but it is essential for the time-dependent problem considered in §5. The new slow variable σ_1 is suggested by the form of h above, and it is defined by

$$\sigma_1 = \epsilon^{\frac{1}{2}}\xi, \tag{14a}$$

which implies that $\sigma = \epsilon^{\frac{1}{2}}\sigma_1$. The new asymptotic scheme is

$$\epsilon^{\frac{1}{2}} \to 0, \quad \sigma_1, \eta \text{ fixed.} \tag{14b}$$

Another expression for h, in terms of σ_1, is necessary (see (27 *c*)).

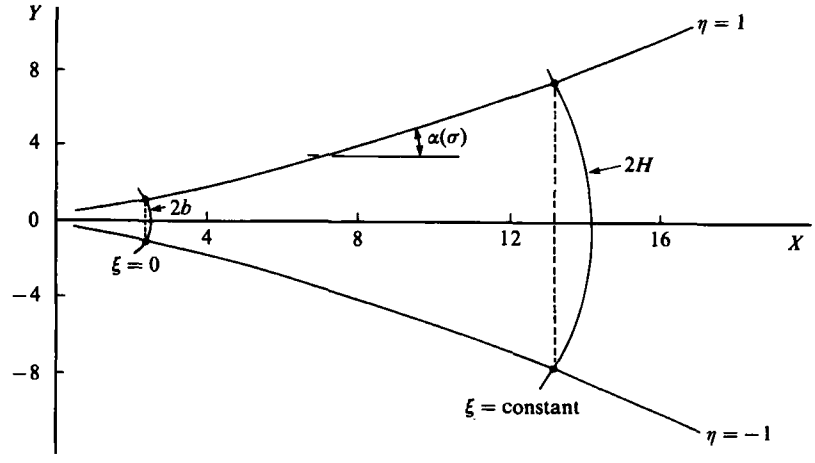

FIGURE 1. A curved-walled channel given by $\alpha(\tau) = \epsilon^{\frac{1}{2}} + \epsilon^{\frac{1}{2}} m\tau$ for $m = 1$ and $\epsilon^{\frac{1}{2}} = 0.4$.

We can obtain an expression for z in terms of σ_1 and η by substituting the relevant parameters in (3) and integrating twice; this yields

$$z = C_1 \int_0^{\zeta} \exp\left(l\epsilon^{\frac{1}{2}} s + \tfrac{1}{2}\epsilon^{\frac{3}{2}} m s^2\right) \mathrm{d}s + C_2. \tag{15}$$

The real constants of integration C_1 and C_2 correspond to different z-scales and choice of origin respectively. On choosing the boundary conditions to be

$$\frac{\mathrm{d}z}{\mathrm{d}\zeta} = 1, \quad z = \frac{1}{\epsilon^{\frac{1}{2}}} \quad (\zeta = 0),$$

we are able to show that (15) reduces to

$$z \sim \exp\left(\sigma_1 + \mathrm{i}\epsilon^{\frac{1}{2}}\eta\right)/\epsilon^{\frac{1}{2}}$$

under the new asymptotic limit given by (14*b*). In fact this particular form of z represents the modified polar coordinates of Eagles (1966, 1973) and Eagles & Weissman (1975, hereinafter referred to as EW) for the straight-walled channel of divergence angle $2\epsilon^{\frac{1}{2}}$.

A plot for this channel is illustrated in figure 1 for the case $m = 1$ and $\epsilon^{\frac{1}{2}} = 0.4$. An exact expression can be found for (15) in the form of a reduction formula, which can then be expanded in ascending powers of $\epsilon^{\frac{1}{2}}$. Alternatively, a Simpson's rule may be adapted for complex functions in the complex plane.

4. The steady-state problem

The equation satisfied by $\Omega(\xi, \eta)$ can be deduced from (5) by letting $\Psi = \Omega(\xi, \eta)$ to obtain

$$\left\{\frac{1}{R}\left(\mathrm{D}^2 - 4\left(\kappa\frac{\partial}{\partial\xi} + \lambda\frac{\partial}{\partial\eta}\right) + 4(\kappa^2 + \lambda^2)\right) - \left(\frac{\partial\Omega}{\partial\eta}\frac{\partial}{\partial\xi} - \frac{\partial\Omega}{\partial\xi}\frac{\partial}{\partial\eta} - 2\kappa\frac{\partial\Omega}{\partial\eta} + 2\lambda\frac{\partial\Omega}{\partial\xi}\right)\right\}\mathrm{D}^2\Omega = 0, \tag{16a}$$

$$\Omega = \pm 1 \quad \text{at } \eta = \pm 1, \quad \frac{\partial\Omega}{\partial\eta} = 0 \quad \text{at } \eta = \pm 1. \tag{16b}$$

We note that (16*a*) is nonlinear, and we assume that Ω is an odd function. This assumption is not implied by the boundary conditions given by (16*b*), but is consistent with those conditions.

Following Fraenkel (1963), the asymptotic expansion for $\Omega(\xi, \eta)$ is assumed to be of the form

$$\Omega(\xi, \eta; v, m) = \Omega_0(\sigma, \eta; v, m) + \epsilon^{\frac{1}{2}}\Omega_1(\sigma, \eta; v, m) + \epsilon\Omega_2(\sigma, \eta; v, m) + \ldots. \tag{17}$$

The necessary expressions for κ and λ in terms of powers of $\epsilon^{\frac{1}{2}}$ can be found from (3) and (12). The equations for Ω_0, Ω_1, Ω_2 etc. can be found by substituting (17) into (16*a*) and comparing powers of $\epsilon^{\frac{1}{2}}$ using $\partial\Omega/\partial\xi = \epsilon\,\partial\Omega/\partial\sigma$. These equations are given in Appendix (1 A).† The new slow variable σ_1 is introduced by expanding each function Ω_0, Ω_1, Ω_2 etc. as a Taylor series about $\sigma = 0$ using $\sigma = \epsilon^{\frac{1}{2}}\sigma_1$. New functions are defined such that

$$\Omega_0(\sigma, \eta; v, m) = G_0(\eta; v) + \epsilon^{\frac{1}{2}}\sigma_1 G_1(\eta; v, m) + \epsilon\sigma_1^2 G_2(\eta; v, m) + \ldots, \tag{18}$$

$$\Omega_1(\sigma, \eta; v, m) = F_0(\eta; v) + \epsilon^{\frac{1}{2}}\sigma_1 F_1(\eta; v, m) + \epsilon\sigma_1^2 G_2(\eta; v, m) + \ldots, \tag{19}$$

$$\Omega_2(\sigma, \eta; v, m) = H_0(\eta; v) + \epsilon^{\frac{1}{2}}\sigma_1 H_1(\eta; v, m) + \epsilon\sigma_1^2 H_2(\eta; v, m) + \ldots, \tag{20}$$

so that now

$$\Omega(\xi, \eta; v, m) = G_0 + \epsilon^{\frac{1}{2}}(F_0 + \sigma_1 G_1) + \epsilon(H_0 + \sigma_1 F_1 + \sigma_1^2 G_2) + \ldots. \tag{21}$$

Of course, this expansion is expected to be useful for $\sigma_1 = O(1)$ with $\epsilon^{\frac{1}{2}}$ small, that is with $\xi = O(1/\epsilon^{\frac{1}{2}})$, as opposed to (17), which would be useful for $\xi = O(1/\epsilon)$. The smaller range of ξ is the price we must pay to perform a stability analysis later.

The relations (18)–(20) are substituted into the equations for Ω_0, Ω_1 and Ω_2, and by comparing powers of $\epsilon^{\frac{1}{2}}$ a set of ξ independent ordinary differential equations is obtained. The equation for G_0 is

$$\frac{\mathrm{d}^4 G_0}{\mathrm{d}\eta^4} + 2vl\frac{\mathrm{d}G_0}{\mathrm{d}\eta}\frac{\mathrm{d}^2 G_0}{\mathrm{d}\eta^2} = 0, \tag{22a}$$

where

$$G_0 = \pm 1, \quad \frac{\mathrm{d}G_0}{\mathrm{d}\eta} = 0 \quad \text{at } \eta = \pm 1. \tag{22b}$$

We note that G_0 is a nonlinear function. For different values of v we obtain a family of velocity profiles $\mathrm{d}G_0/\mathrm{d}\eta$, some of these with reversed flow near $\eta = \pm 1$. This equation for G_0 is identical with the equation for G defined by Fraenkel (1962, (2.1*a*)) with $\alpha \to 0$ and $R\alpha$ fixed. Any observed reverse flow is regular; that is, separation and reattachment can occur without singularities (Fraenkel 1962, p. 133).

The full equations satisfied by G_1, G_2, F_0, F_1 and H_0 are stated in Appendix (1 B). They have a general form, which may be expressed as

$$\frac{\mathrm{d}^4\chi}{\mathrm{d}\eta^4} + 2vl\frac{\mathrm{d}}{\mathrm{d}\eta}\left(\frac{\mathrm{d}G_0}{\mathrm{d}\eta}\frac{\mathrm{d}\chi}{\mathrm{d}\eta}\right) = \mathscr{D}, \tag{23a}$$

where

$$\chi = \frac{\mathrm{d}\chi}{\mathrm{d}\eta} = 0 \quad \text{at } \eta = \pm 1. \tag{23b}$$

The equations are linear, and $\mathscr{D}$ is different for each function. The assumption that Ω is odd implies symmetric velocity profiles for the steady-state flow.

† All the Appendices are kept in the Editorial Office and may be obtained on request to the Editor.

	$v = 3.572$ $R = 30$, $\epsilon^{\frac{1}{2}} = 0.19$		$v = 4.71$ $R = 10.5$, $\epsilon^{\frac{1}{2}} = 0.449$	
η	G_0'	$G_0'+\epsilon H_0'$	G_0'	$G_0'+\epsilon H_0'$
0	1.856	1.860	2.187	2.339
0.1	1.813	1.817	2.113	2.251
0.2	1.691	1.694	1.906	2.005
0.3	1.504	1.505	1.604	1.650
0.4	1.273	1.273	1.256	1.248
0.5	1.021	1.019	0.9069	0.8555
0.6	0.7682	0.7657	0.5934	0.5143
0.7	0.5309	0.5279	0.3375	0.2494
0.8	0.3200	0.3172	0.1509	0.0729
0.9	0.1420	0.1402	0.079	−0.0106
1.0	0	0	0	0

TABLE 1. The steady-state velocity profiles with and without the $O(\epsilon)$ correction for different straight-walled channels ($m = 0$)

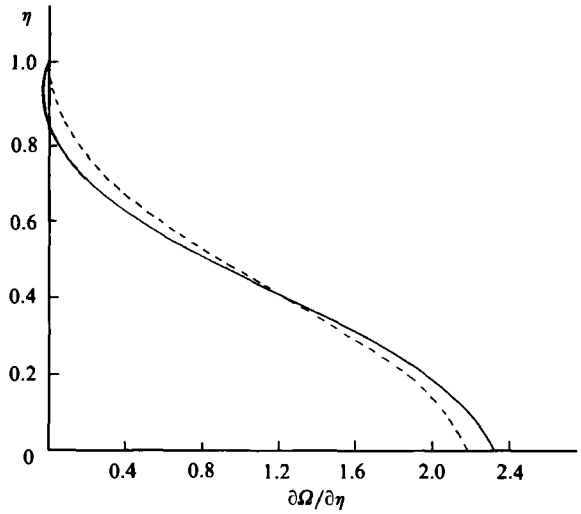

FIGURE 2. The effect of the $O(\epsilon)$ correction to the steady-state velocity profile in the straight-walled channel for $v = 4.71$, $R = 10.5$: ----, $O(1)$; ——, $O(\epsilon)$.

The scheme to solve for G_0 is essentially a perturbation about Poiseuille flow. The function is expressed as an ascending power series in v:

$$G_0 = \sum_{r=0}^{\infty} w_r v^r. \tag{24}$$

This scheme has two important advantages. The first is that the perturbation functions w_r are unique and need only be computed once. The second is that the resulting matrix equation defining w_r need only be modified marginally in order to incorporate it for solving (23a). Details of this perturbation scheme and numerical checks on the accuracy of the asymptotic expansion (17) can be found in Georgiou & Ellinas (1985).

The range of v considered ($0 \leqslant v \leqslant 5$) is necessarily restricted (Fraenkel 1962) to

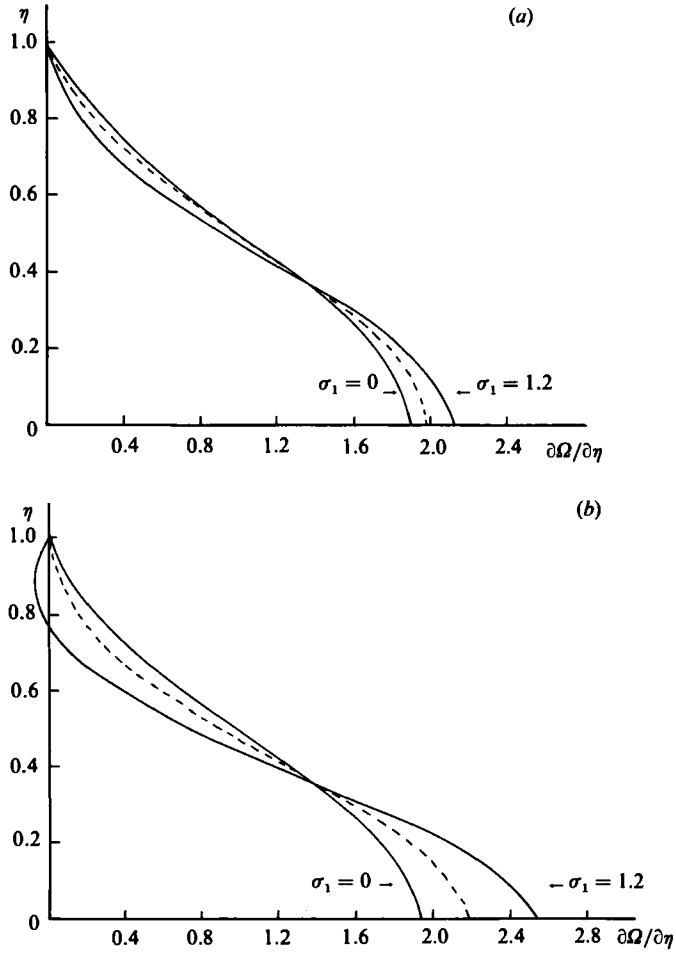

FIGURE 3. The transverse behaviour of the steady-state profile for the curved- ($m = 1$) and straight-walled ($m = 0$) channels, at different positions downstream, with (*a*) $v = 4.093$, $R = 30$; (*b*) $v = 4.71$, $R = 30$: ----, $m = 0$; ——, $m = 1$.

ensure that G_0 is unique, and at most one region of reversed flow is observed near the walls of the channel.

The divergent or convergent plane-walled channel (straight-walled) solution may be retrieved asymptotically, $\epsilon \to 0$, σ_1, η and m fixed or by letting $m = 0$. The simplified system with $m = 0$ leads to

$$\Omega = G_0 + \epsilon H_0 + \ldots, \tag{25}$$

where $G_1 = G_2 = F_0 = F_1 = 0$ satisfy (23*a*). The effect, as a result of including the higher-order term ϵH_0, is probably best described using the velocity profile $\partial\Omega/\partial\eta$. The results in table 1 demonstrate the tendency of increased velocity at the centre and decreased velocity near the walls. In an extreme case of $v = 4.71$ and $R = 10.5$ some reversed flow is observed with this additional term, and this is illustrated in figure 2. The additional term corresponds to the $O(\alpha^2)$ term omitted by EW. The terms G_0' and H_0' represent derivatives with respect to η in table 1.

The effects of curvature are realized by a comparison between the velocity profiles

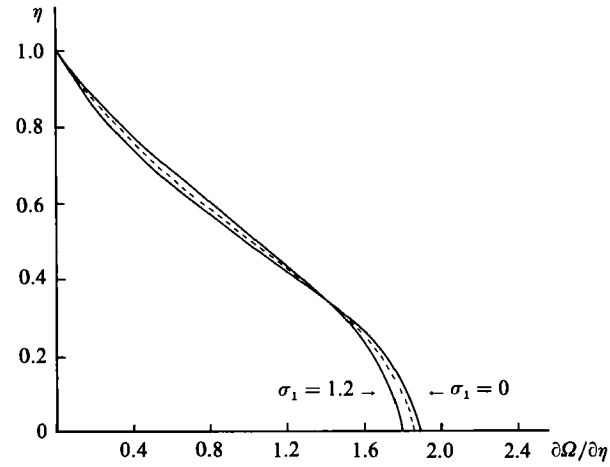

FIGURE 4. The transverse behaviour of the steady-state profile for the curved- ($m = -1$) and straight-walled ($m = 0$) channels, at different positions downstream, with $v = 3.572$ and $R = 30$: ----, $m = 0$; ——, $m = -1$.

in straight- and curved-walled channels. These are illustrated in figures 3 (a, b), where velocity profiles, at different downstream positions, for the case $m = 1$, are compared with those for the case $m = 0$. We note that, at $\sigma_1 = 0$, the angle of divergence is the same for both the straight- and curved-walled channels, and the $O(\epsilon)$ correction is included. At $\sigma_1 = 0$, when $m > 0$ the velocity at the centre tends to decrease, while at the walls the velocity tends to increase. This is precisely the opposite effect of the higher-order terms. However, as we move downstream, these dominant curvature effects increase the velocity at the centre and decrease it near the walls. This somewhat surprising result at $\sigma_1 = 0$ may be explained in the following way. If $m > 0$ then the angle of divergence is greater than in the corresponding straight-walled case for $\sigma_1 > 0$. Similarly it is less for $\sigma_1 < 0$. The velocity for $m > 0$ and $\sigma_1 < 0$ is then expected to be smaller at the centre than its straight-walled counterpart. Upstream influence causes this to persist to $\sigma_1 = 0$ and possibly a little beyond. If this were the case we might then expect the opposite to happen at $\sigma_1 = 0$ when $m < 0$. The graph in figure 4, for the case $m = -1$, shows this to be so.

5. The time-dependent problem

We now set $\Psi(\xi, \eta, t) = \Omega(\xi, \eta) + \Phi(\xi, \eta, t)$ and linearize Φ to obtain

$$\left\{\frac{1}{R}\left(\mathrm{D}^2 - 4\left(\kappa\frac{\partial}{\partial\xi} + \lambda\frac{\partial}{\partial\eta}\right) + 4(\kappa^2+\lambda^2)\right) - h^2\frac{\partial}{\partial t} - \left(\frac{\partial\Omega}{\partial\eta}\frac{\partial}{\partial\xi} - \frac{\partial\Omega}{\partial\xi}\frac{\partial}{\partial\eta} - 2\kappa\frac{\partial\Omega}{\partial\eta} + 2\lambda\frac{\partial\Omega}{\partial\xi}\right)\right\}\mathrm{D}^2\Phi$$
$$-\left(\frac{\partial\Phi}{\partial\eta}\frac{\partial}{\partial\xi} - \frac{\partial\Phi}{\partial\xi}\frac{\partial}{\partial\eta} - 2\kappa\frac{\partial\Phi}{\partial\eta} + 2\lambda\frac{\partial\Phi}{\partial\xi}\right)\mathrm{D}^2\Omega = 0, \quad (26a)$$

where
$$\Phi = \frac{\partial\Phi}{\partial\eta} = 0 \quad \text{at } \eta = \pm 1. \quad (26b)$$

We take Φ to be even in η, since this is generally known to produce the most-unstable disturbances. The coefficients of (26a) are independent of time and are slowly varying with ξ; therefore the stream function of the disturbance for constant frequencies β

may be chosen to be of the form

$$\Phi(\xi,\eta,t) = \phi(\sigma_1,\eta)\exp(\mathrm{i}[\theta(\xi)-\beta t])+\text{c.c.}, \tag{27a}$$

where c.c. represents the complex conjugate of the preceding term, and β is chosen to be real. The slow variation of the coefficients in the ξ-direction is allowed for by the complex wavenumber $k(\sigma_1)$, which is defined in terms of the complex phase function $\theta(\xi)$, where

$$\frac{\mathrm{d}\theta}{\mathrm{d}\xi} = k(\sigma_1). \tag{27b}$$

The necessary expression for h in powers of $\epsilon^{\frac{1}{3}}$ is established by integrating (3) with the boundary conditions $\mathrm{d}z/\mathrm{d}\zeta = 1$ at $\zeta = 0$ and comparing with (2). In this case it is exact and is given by

$$h = \exp[l\sigma_1+\tfrac{1}{2}\epsilon^{\frac{1}{3}}m\sigma_1^2-\tfrac{1}{2}m\epsilon^{\frac{2}{3}}\eta^2]. \tag{27c}$$

In the steady-state case a certain condition is imposed on R and $\epsilon^{\frac{1}{3}}$, (13a). This condition is relaxed for the time-dependent analysis. Now R and $\epsilon^{\frac{1}{3}}$ are treated as independent parameters in the asymptotic development, but (13a) is returned to in the final analysis of the results. This technique has already been used extensively by other authors (EW; Gaster 1974; Bouthier 1972, 1973; Ling & Reynolds 1973; Lanchon & Eckhaus 1964; Eagles & Smith 1980), where supportive arguments are given for this relaxation. Also, Allmen (1980) has shown the procedure to be accurate for certain channel flows by an independent numerical method. The alternative approach, of retaining the condition, leads to a singular perturbation problem of extreme complexity, and, although the present method is difficult to justify theoretically (see EW for an elementary example of how it works), we feel that its use is justified in the light of supporting and consistent results of the other workers cited above. We continue the asymptotic development and use

$$\phi(\sigma_1,\eta;R,v,m) = \phi_0(\sigma_1,\eta;R,v,m)+\epsilon^{\frac{1}{3}}\phi_1(\sigma_1,\eta;R,v,m)+\epsilon\phi_2(\sigma_1,\eta;R,v,m)+\ldots. \tag{28}$$

The function ϕ is conveniently and arbitrarily normalized by $\phi(0,0) = 1$. This is equivalently expressed as

$$\phi_0(0,0) = 1, \quad \phi_i(0,0) = 0, \quad i \geqslant 1. \tag{29}$$

Substituting (28) into (26a) and comparing powers of $\epsilon^{\frac{1}{3}}$, the following set of equations is obtained:

$$\mathrm{L}\phi_0 = 0, \tag{30a}$$

where

$$\phi_0(\sigma_1,\pm 1) = \frac{\partial\phi_0}{\partial\eta}(\sigma_1,\pm 1) = 0, \tag{30b}$$

$$\mathrm{L} \equiv \frac{1}{R}(\mathrm{D}_1^2-k^2)^2+\mathrm{i}\left(\beta_{\mathrm{I}}-k\frac{\mathrm{d}G_0}{\mathrm{d}\eta}\right)(\mathrm{D}_1^2-k^2)+\mathrm{i}k\frac{\mathrm{d}^3G_0}{\mathrm{d}\eta^3}, \tag{30c}$$

$$\beta_{\mathrm{I}} = \beta\mathrm{e}^{2l\sigma_1}, \quad \mathrm{D}_1^2 = \frac{\partial^2}{\partial\eta^2}. \tag{30d}$$

This equation at $O(1)$ represents the classic Orr–Sommerfeld problem, in which the frequency and wavenumber are replaced by functions of the slow variable σ_1. For a given β (real) and fixed σ_1 it is an eigenvalue problem in k. The $O(\epsilon^{\frac{1}{3}})$ equation is

$$\mathrm{L}\phi_1 = \mathrm{L}_1\frac{\partial\phi_0}{\partial\sigma_1}+\frac{\mathrm{d}k}{\mathrm{d}\sigma_1}\mathrm{L}_2\phi_0+(\mathrm{L}_3+\mathrm{L}_4)\phi_0, \tag{31a}$$

where $$\phi_1(\sigma_1, \pm 1) = \frac{\partial \phi_1}{\partial \eta}(\sigma_1, \pm 1) = 0. \tag{31b}$$

The additional operators L_1, L_2, L_3 and L_4 are defined in Appendix (2 A). It is interesting at this stage to note that the term $\beta_I i m \sigma_1^2$ in L_3 and L_4 is a direct consequence of curvature, and would disappear on setting $m = 0$. For this case L, L_1, L_2 and L_3 become the operators for the straight-walled channel, and are the same operators defined in the investigation by EW. Continuing to the $O(\epsilon)$ equation, we obtain

$$\begin{aligned} L\phi_2 = L_1 \frac{\partial \phi_1}{\partial \sigma_1} + \frac{dk}{d\sigma_1} L_2 \phi_1 + (L_3 + L_4)\phi_1 + (M_1 + M_2)\frac{\partial \phi_0}{\partial \sigma_1} + \frac{dk}{d\sigma_1}(M_3 + M_4)\phi_0 \\ + \frac{dk}{d\sigma_1} M_5 \frac{\partial \phi_0}{\partial \sigma_1} + \left(M_6 + M_7 + M_8 + \frac{d^2k}{d\sigma_1^2}\left(4\kappa + i\frac{dG_0}{d\eta}\right) + \frac{3}{R}\left(\frac{dk}{d\sigma_1}\right)^2 \right)\phi_0 - iL_2 \frac{\partial^2 \phi_0}{\partial \sigma_1^2}, \end{aligned} \tag{32a}$$

where $$\phi_2(\sigma_1, \pm 1) = \frac{\partial \phi_2}{\partial \eta}(\sigma_1, \pm 1) = 0. \tag{32b}$$

The extra operators $M_1, \ldots, M_8$ are a direct consequence of curvature and higher-order terms from the steady-state analysis. Some of these will simplify a great deal upon setting $m = 0$, while others will vanish completely. They are defined in Appendix (2 B). We note that (32*a*) was not established by EW for their straight-walled case.

From the theory of homogeneous equations a characteristic equation (eigenrelation) must be satisfied for the existence of a non-trivial solution. This eigenrelation, $k(\sigma_1) = F(\beta_I, R, v)$, forms the basis for any iterative schemes to compute the eigenvalues (Georgiou & Ellinas 1985).

The variable σ_1 appears only as a parameter in (30*a*), and hence a solution may be found in the form

$$\phi_0(\sigma_1, \eta) = A_0(\sigma_1) f_0(\sigma_1, \eta), \tag{33}$$

where A_0 is called the amplitude, and the eigenfunction f_0 is a solution to (30*a*) using (30*b*) for some fixed σ_1. We normalize f_0 arbitrarily following (29), and choose

$$f_0(\sigma_1, 0) = 1 \quad \text{for all } \sigma_1. \tag{34}$$

With this normalization the complex function A_0 may be interpreted as the amplitude of ϕ_0 along the centre of the channel, but it is not the total amplitude. A different normalization of f_0 would correspond to a different interpretation for A_0.

A Runge–Kutta scheme of order four is used to solve the homogeneous equation (30*a*) after the eigenvalues have been evaluated. To solve for A_0 we need to go to the $O(\epsilon^{\frac{1}{2}})$ disturbance equation (31*a*). It can be shown that for a solution to exist

$$\int_{-1}^{1} \tilde{f}_0 L\phi_1 \, d\eta = 0, \tag{35}$$

where $\tilde{f}_0$ is the adjoint eigenfunction (Ince 1956). Using (33) and the solvability condition (35), we find

$$\frac{dA_0}{d\sigma_1} + H(\sigma_1) A_0 = 0, \tag{36a}$$

where (29) and (34) imply

$$A_0(0) = 1. \tag{36b}$$

The complex function $H(\sigma_1)$ is defined in terms of definite integrals, and these are stated in Appendix (2 A). The solution of the non-homogeneous equations (31 *a*) and (32 *a*) can be expressed in terms of the previous homogeneous solution. The stream functions ϕ_1, ϕ_2 may be put in the form

$$\phi_i(\sigma_1, \eta) = f_i(\sigma_1, \eta) + A_i(\sigma_1) f_0(\sigma_1, \eta), \quad i \geqslant 1, \tag{37a}$$

where

$$f_i(\sigma_1, \pm 1) = \frac{\partial f_i}{\partial \eta}(\sigma_1, \pm 1) = 0, \quad i \geqslant 1. \tag{37b}$$

If we wish to interpret $A_i(\sigma_1)$, $i \geqslant 1$, as the amplitude of $\phi_i(\sigma_1, \eta)$ along the centre of the channel, then the normalizations on $f_i(\sigma_1, \eta)$ are clear. All physical quantities such as growth rates (to be defined in §6) are unaffected by these arbitrary normalizations. As before, different normalizations on $f_i(\sigma_1, \eta)$ merely correspond to different $A_i(\sigma_1)$. Thus we choose

$$f_i(\sigma_1, 0) = 0, \quad i \geqslant 1, \quad \text{for all } \sigma_1. \tag{38}$$

The functions f_1 and f_2 satisfy (31 *a*) and (32 *a*) respectively. The necessary eigenrelation for the homogeneous system implies that $f_i(\sigma_1, \eta)$ are not unique solutions. In fact an infinity of solutions exist for each $f_i(\sigma_1, \eta)$, and only particular solutions may be found.

In order to solve for any $A_i(\sigma_1)$ it is always necessary to go to the next-order equation and apply the solvability condition

$$\int_{-1}^{1} f_0 \, \mathrm{L}\phi_{i+1} \, \mathrm{d}\eta = 0, \quad i \geqslant 1, \tag{39}$$

as before. We find by substituting (37 *a*) into the appropriate non-homogeneous equation and using (39) that

$$\frac{\mathrm{d}A_i}{\mathrm{d}\sigma_1} + H(\sigma_1) \, A_i = \mathscr{F}_i(\sigma_1), \quad i \geqslant 1, \tag{40a}$$

where

$$A_i(0) = 0, \quad i \geqslant 1. \tag{40b}$$

For this analysis it is only necessary to go as far as A_1. The function $\mathscr{F}_i(\sigma_1)$ is defined for the case $i = 1$ in Appendix (2 B); it becomes obvious that for each amplitude function an increasing number of integrals are introduced as a result of new operators appearing in each higher-order non-homogeneous equation.

Numerical checks were first carried out on f_0 and A_0; these were also computed by EW for the straight-walled channel. In addition to these, the independent checks on f_0 and its derivatives, carried out on the boundary, showed self-consistency. The further extensive checks on f_1 and A_1, which were not computed by EW for the straight-walled channel, validated the work so far. It is worth noting that when f_1 is correct it serves as a check on A_0. Hence one important check on A_1 would be to solve (32 *a*) for the function f_2. This lengthy equation was solved for this purpose, and the checks proved conclusive.

6. The growth rates

Quasiparallel theory says that each flow quantity (stream function, velocity etc.) has the same constant growth rate, and this is equal to $-k_{\mathrm{i}}$ (k_{i} is the imaginary part of k). The theory can only tell us whether a wave is growing or decaying at a particular

point and not as function of the downstream variable (EW). In this analysis, as in EW, k_1 is a function of the downstream variable, and, because of the inclusion of higher-order terms, different flow quantities have different growth rates. We define the spatial growth rate for any flow quantity (such as stream function and velocity components) by

$$\mathrm{GR}_\xi(Q) = (\mathrm{amp}\, Q)^{-1} \frac{\partial}{\partial \xi} (\mathrm{amp}\, Q), \tag{41}$$

and with this definition we find that $-k_1(\sigma_1)$ appears as the first-order term. The fact that different flow quantities have different growth raises the question: 'What gives a "true" measure of the growth of a disturbance?'

Shen (1961) gives an intuitive argument as to what 'yardstick' could be used to measure the growth or decay of a disturbance. A disturbance that appears to be growing might actually be decaying if it is measured relative to a base flow that is growing at a faster rate. A similar reasoning may apply for a disturbance that appears to be decaying (Lin 1951). This argument suggests that, in the case of measuring the growth of a wave based on a mean kinetic-energy density E, a more appropriate measurement is a relative mean kinetic-energy density $\hat{E}$, where

$$\hat{E} = E/E_0, \tag{42}$$

and E_0 is the kinetic-energy density of the basic flow. This idea is adapted for our spatially dependent basic flow.

We define a mean kinetic-energy density per unit width in the streamwise direction, which is averaged over time and integrated across the channel (EW). It is expressed by

$$E = \frac{1}{2} \int_{-1}^{1} h(\overline{u_\xi^2} + \overline{u_\eta^2})\, \mathrm{d}\eta, \tag{43}$$

where $\overline{u_\xi^2}$ and $\overline{u_\eta^2}$ are the mean-square velocities in the streamwise and transverse directions respectively. The scaling factor h, given by (27c), is used along with (27a) to establish expressions for u_ξ and u_η in terms of ϕ, since

$$u_\xi = \frac{1}{h} \frac{\partial \Phi}{\partial \eta}, \quad u_\eta = -\frac{1}{h} \frac{\partial \Phi}{\partial \xi}. \tag{44}$$

From these expressions we can find the square of the velocities and the mean-square velocities averaged over one period π/β, these are

$$\overline{u_\xi^2} = 2\, \mathrm{e}^{-2l\sigma_1} (1 - m\epsilon^{\frac{1}{2}}\sigma_1^2 + \tfrac{1}{2}m^2\epsilon\sigma_1^4) \left|\frac{\partial \phi}{\partial \eta}\right|^2 \mathrm{e}^{-2\theta_1} + \ldots, \tag{45a}$$

$$\overline{u_\eta^2} = 2\, \mathrm{e}^{-2l\sigma_1} (1 - m\epsilon^{\frac{1}{2}}\sigma_1^2 + \tfrac{1}{2}m^2\epsilon\sigma_1^4) \left|ik\phi + \epsilon^{\frac{1}{2}} \frac{\partial \phi}{\partial \sigma_1}\right| \mathrm{e}^{-2\theta_1} + \ldots. \tag{45b}$$

Hence

$$E = \mathrm{e}^{-l\sigma_1}\, \mathrm{e}^{-2\theta_1} (1 - \tfrac{1}{2}m\epsilon^{\frac{1}{2}}\sigma_1^2 + \tfrac{1}{8}m^2\epsilon\sigma_1^4)\, S_1, \tag{46}$$

where

$$S_1(\sigma_1) = \int_{-1}^{1} \left(\left|\frac{\partial \phi}{\partial \eta}\right|^2 + \left|ik\phi + \epsilon^{\frac{1}{2}} \frac{\partial \phi}{\partial \sigma_1}\right| \right) \mathrm{d}\eta. \tag{47}$$

The growth rate of E, $\mathrm{GR}_\xi(E)$, is defined using (41), but a factor of $\frac{1}{2}$ is necessary to ensure that $-k_1(\sigma_1)$ appears at $O(1)$. Thus

$$\mathrm{GR}_\xi(E) = \tfrac{1}{2} E^{-1} \frac{\mathrm{d}E}{\mathrm{d}\xi}. \tag{48}$$

Hence
$$\mathrm{GR}_\xi(E) = -k_1 + \epsilon^{\frac{1}{2}}\left(-\tfrac{1}{2} + \frac{\mathrm{d}S_1}{\mathrm{d}\sigma_1}\Big/S_1\right) - \tfrac{1}{2}\epsilon m\sigma_1 + \ldots. \tag{49}$$

We note that, since ϕ in (45a, b) and S_1 contain powers of $\epsilon^{\frac{1}{2}}$, (45a, b) and (49) are not strictly in ascending powers of $\epsilon^{\frac{1}{2}}$. E_0 is given by

$$E_0 = \frac{1}{2}\int_{-1}^{1} h(v_\xi^2 + v_\eta^2)\,\mathrm{d}\eta, \tag{50}$$

where the streamwise and transverse velocities v_ξ and v_η respectively are given by

$$v_\xi = \frac{1}{h}\frac{\partial\Omega}{\partial\eta}, \quad v_\eta = -\frac{1}{h}\frac{\partial\Omega}{\partial\xi}. \tag{51}$$

By expressing these in ascending powers of $\epsilon^{\frac{1}{2}}$ and substituting into (50), we obtain

$$E_0 = \mathrm{e}^{-l\sigma_1}[1 - \tfrac{1}{2}m\epsilon^{\frac{1}{2}}\sigma_1^2 + \tfrac{1}{8}m^2\epsilon\sigma_1^4]\,\Gamma, \tag{52a}$$

where
$$\Gamma(\sigma_1) = \frac{1}{2}\int_{-1}^{1}\left[\left(\frac{\mathrm{d}G_0}{\mathrm{d}\eta}\right)^2 + \epsilon^{\frac{1}{2}}\frac{\mathrm{d}G_0}{\mathrm{d}\eta}\left(\frac{\mathrm{d}F_0}{\mathrm{d}\eta} + \sigma_1\frac{\mathrm{d}G_1}{\mathrm{d}\eta}\right)\right]\mathrm{d}\eta. \tag{52b}$$

Using (42), (46) and (52), we obtain

$$\hat{E} = \frac{S_1}{\Gamma}\,\mathrm{e}^{-2\theta_1}. \tag{53}$$

Using (48) to define $\mathrm{GR}_\xi(\hat{E})$, we have for the 'true' measure of the disturbance

$$\mathrm{GR}_\xi(\hat{E}) = -k_i + \epsilon^{\frac{1}{2}}\frac{\mathrm{d}S_1}{\mathrm{d}\sigma_1}\Big/2S_1 - \epsilon\frac{\mathrm{d}\Gamma_2}{\mathrm{d}\sigma_1}\Big/2\Gamma_1 + \ldots, \tag{54}$$

where
$$\frac{\mathrm{d}\Gamma_2}{\mathrm{d}\sigma_1} = \int_{-1}^{1}\frac{\mathrm{d}G_0}{\mathrm{d}\eta}\frac{\mathrm{d}G_1}{\mathrm{d}\eta}\mathrm{d}\eta, \tag{55a}$$

$$\Gamma_1 = \frac{1}{2}\int_{-1}^{1}\left(\frac{\mathrm{d}G_0}{\mathrm{d}\eta}\right)^2\mathrm{d}\eta. \tag{55b}$$

Direct comparisons can be made between (52)–(55) and the corresponding expressions in EW. To do this requires expressions in ascending powers of $\epsilon^{\frac{1}{2}}$ explicitly up to the term in $\epsilon^{\frac{1}{2}}$ (EW did not establish the $O(\epsilon)$ term). These explicit forms are derived from the equations above, and on setting $m = 0$ they agree identically with those in EW.

7. The results of the numerical calculations

First, in the case of $m = 0$ the present work represents an extension and a check on the work of EW to the next-order term. Such an extension is important because k_i is numerically small and it is not certain that a series for the growth rates to $O(\epsilon^{\frac{1}{2}})$ is sufficiently accurate.

We plot values of $\mathrm{GR}_\xi(\hat{E})$ against β_I. This enables us to choose and determine the range of frequencies for which $\mathrm{GR}_\xi(\hat{E}) > 0$. In figure 5 we see the effect of increasing R for a particular v. When $R = 30$ the curve does not cross the β_I axis, thus $\mathrm{GR}_\xi(\hat{E}) < 0$ for all β_I. On the other hand, when $R = 50$, $\mathrm{GR}_\xi(\hat{E}) > 0$ between A and B. We note that, when $m = 0$, β and σ_1 always appear together in the form of β_I. Thus by arbitrarily choosing σ_1 we can determine the range of β for which we

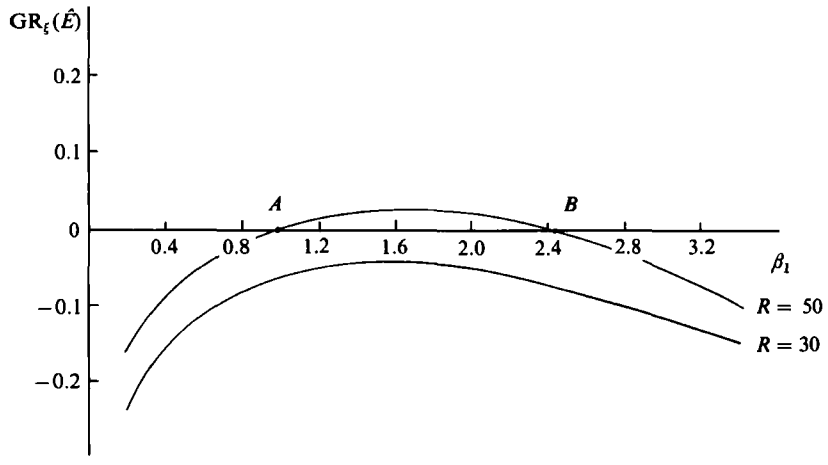

FIGURE 5. The general behaviour of the relative kinetic energy with the intrinsic frequency in a straight-walled channel, for increased Reynolds number, with $v = 3.572$.

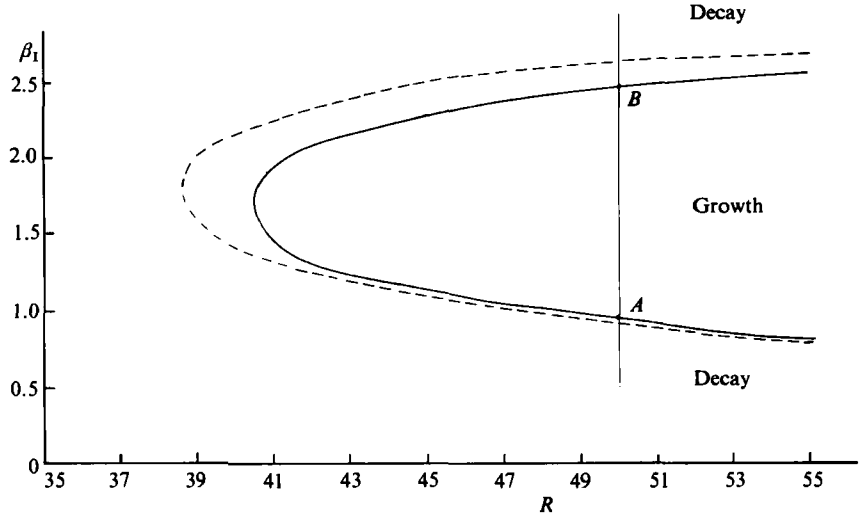

FIGURE 6. Neutral-stability curves at different orders for the straight-walled channel ($m = 0$) with $v = 3.572$: ——, EW; ——, $O(\epsilon)$ correction.

can expect growth. Similarly, by arbitrarily choosing a frequency β we can determine the range of σ_1 for which we can expect growth.

The positions A and B in figure 5 define 'critical' points for fixed v and R. By taking different values of R, a set of critical points contribute to form a 'neutral' curve. This procedure may be carried out for both the $O(\epsilon^{\frac{1}{2}})$ and $O(\epsilon)$ forms of $GR_\xi(\hat{E})$. In figure 6 a comparison is made between two neutral curves corresponding to the $O(\epsilon^{\frac{1}{2}})$ and $O(\epsilon)$ forms of $GR_\xi(\hat{E})$. Note that A and B in figure 5 are identified in figure 6. As we move up the line joining AB produced (fixed R) we are initially in a region of decay, then a region of growth, and finally a region of decay. These neutral curves each define a critical Reynolds number R_c. If $R > R_c$ the disturbance grows for fixed frequencies, albeit for a limited range of σ_1 values, and we say the flow is unstable in this sense.

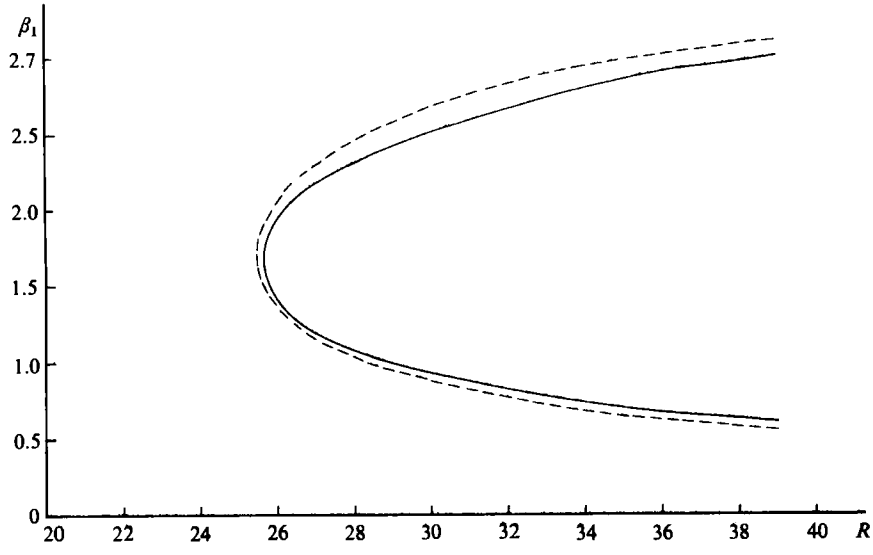

FIGURE 7. As figure 6, but with $v = 4.093$.

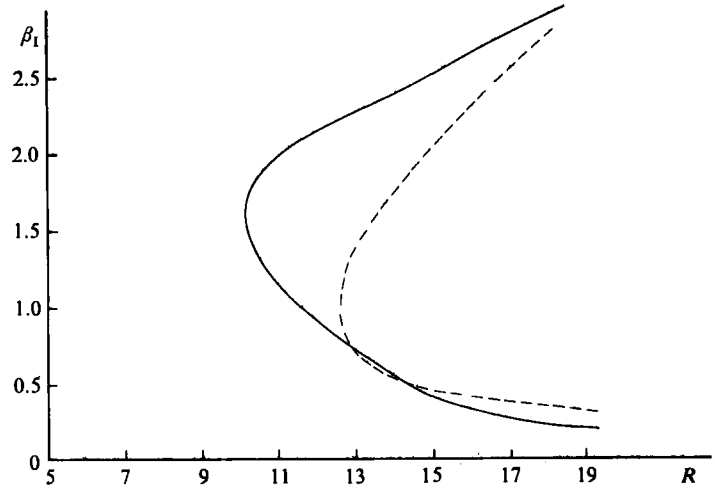

FIGURE 8. As figure 6, but with $v = 4.71$.

On the other hand, if $R < R_c$ the disturbance decays for all frequencies and for all σ_1 values, and we say the flow is stable in this sense.

Further graphs (figures 7 and 8) are included to show the effect of increasing v. These show that some critical v exists, v_c, about which the addition of higher-order terms make the flow more stable when $v < v_c$, and more unstable when $v > v_c$. A set of points (R_c, v) can be established from such graphs, and some of these are tabulated in table 2. By plotting a graph of this table (figure 9) we can establish boundary curves for the $O(\epsilon^{\frac{1}{3}})$ and $O(\epsilon)$ solutions. We return to the relationship (13a) between R and $\epsilon^{\frac{1}{3}}$ in order to interpret the results illustrated in figure 9. Take as an example $\epsilon^{\frac{1}{3}} = 0.1$. As we move along the line defined by this $\epsilon^{\frac{1}{3}}$, the combinations of R_c and v to the

v	R_c, $O(\epsilon^{\frac{1}{3}})$	R_c, $O(\epsilon)$
3.572	38.6	40.5
3.8	32.3	33.4
4.093	25.4	25.5
4.5	16.6	15.2
4.71	12.6	10.2

TABLE 2. Values of R_c, for a range of v in a straight-walled channel ($m = 0$), with and without the $O(\epsilon)$ correction

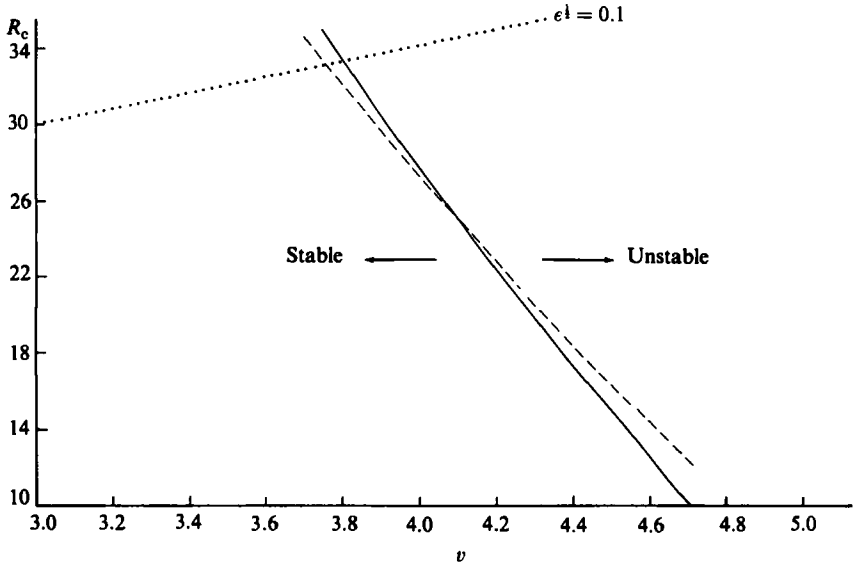

FIGURE 9. Boundary curves separating stable and unstable flow at different orders for the straight-walled channel: ----, EW; ——, $O(\epsilon)$ correction.

left of the boundary curves represent stable flow in the manner already described. Similarly, all points to the right represent unstable flow. The frequencies and positions may be established from curves such as those in figures 6–8. Allmen's (1980) direct numerical attack on the problem of EW could be considered as the most accurate solution. Allmen did not provide a graph of R_c versus v, but rather R versus $\epsilon^{\frac{1}{3}}$. A graph of R_c versus v could nevertheless be plotted from Allmen's results, and it shows the same feature as that illustrated in figure 9, but not as pronounced. This feature is not really noticeable when R_c is plotted against $\epsilon^{\frac{1}{3}}$, but it does exist. The destabilizing effect at larger values of v, due to higher-order terms, is interesting, as it is consistent with the reversed-flow effect they had on the steady-state velocity profile as illustrated in figure 2. These higher-order terms, however, make comparatively little difference to the stability properties. This is in fact fairly surprising when one considers the relatively high values of $\epsilon^{\frac{1}{3}}$ used ($\epsilon^{\frac{1}{3}} = 0.46$ in some cases). These results together with those of Allmen (1980) contribute a convincing check on the results of EW.

Secondly, we consider the case when $m \neq 0$, and we must try to imagine the physical situation when interpreting or using the results. Our channel is part of a much

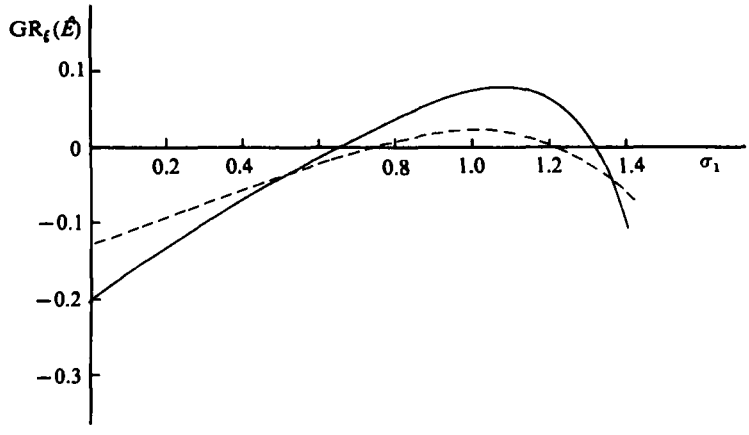

FIGURE 10. The downstream development of the relative kinetic energy for the curved-walled channel ($m = 1$) with $v = 4.093$, $R = 30$, $\beta = 0.2$: ----, $m = 0$; ——, $m = 1$.

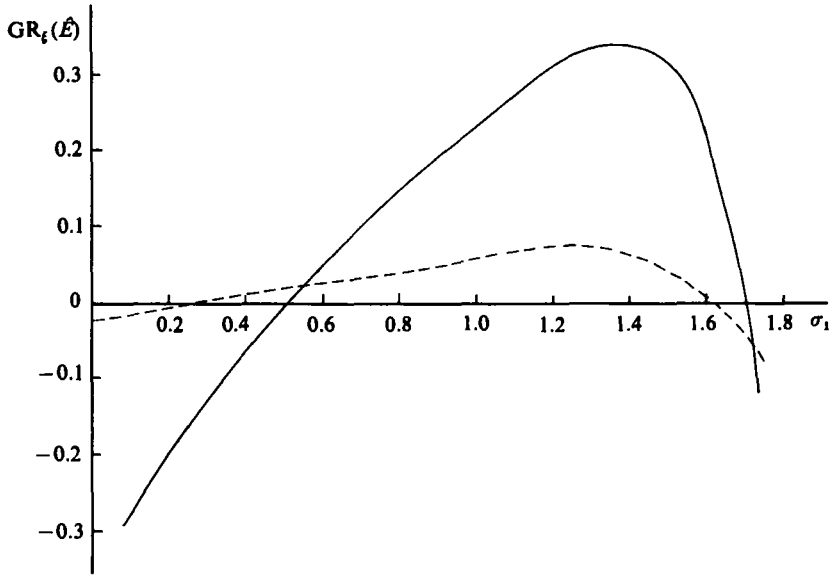

FIGURE 11. As figure 10, but with $v = 4.71$, $R = 20$, $\beta = 0.12$.

larger channel, and, whereas the angle of divergence varies from point to point, the curvature is in fact either always positive or negative. A channel whose curvature varies in sign is considered in §8. The results are essentially local results, but they do take into account curvature and downstream development. These results are much more realistic than those predicted by a purely local quasiparallel theory. In the case of $m = 0$, R_c is the same at all σ_1 stations because β and σ_1 always appear together as β_I. This is not the case when $m \neq 0$, since β and σ_1 can appear independently as well as in the form β_I.

We ask two questions: (i) 'If the curved-walled channel has the same local angle of divergence as a wedge ($m = 0$), is the flow locally more or less stable than the wedge flow?' (ii) 'Is the wedge approximation reasonable for a channel with small wall

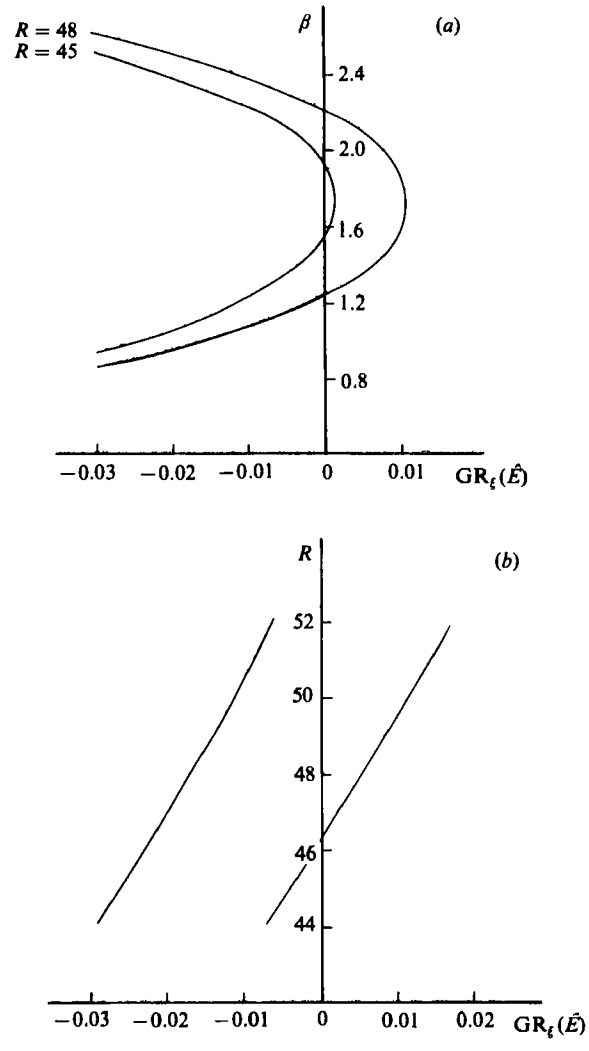

FIGURE 12. The behaviour of the relative kinetic energy with Reynolds number and frequency, for the curved-walled channel ($m = 1$) at $\sigma_1 = 0$ with $v = 3.572$.

curvature?' To answer these questions, we compare the growth rates at $\sigma_1 = 0$ between the cases $m = 0$ and $m \neq 0$.

For the case $m = 1$ and $\sigma_1 \approx 0$ figures 10 and 11 show that $\mathrm{GR}_\xi(\hat{E})$ is numerically smaller than for the corresponding case $m = 0$. This is consistent with the effect of curvature on the basic flow, as illustrated in figure 3(*a*). To be more definite as to which case is more stable at $\sigma_1 = 0$, we may compare R_c values. In the curved-walled channel this needs to be carried out specifically in the plane $\sigma_1 = 0$. Plotting β versus $\mathrm{GR}_\xi(\hat{E})$ (figure 12*a*) for fixed R at $\sigma_1 = 0$, and R versus $\mathrm{GR}_\xi(\hat{E})$ (figure 12*b*) for fixed β at $\sigma_1 = 0$, the behaviour is clear. We require the combination of R and β (R_c, β_c) in which the curve in figure 12(*a*) just touches the β-axis. An interpolation/extrapolation routine is used in which the initial guesses are given by (R, β) at $\sigma_1 = 0$ for the corresponding straight-walled case. Starting off with this initial set of (R_c, β_c) and two other arbitrary values of β (centred on β_c), the corresponding values of $\mathrm{GR}_\xi(\hat{E})$

v	R_c $m = 0$	R_c $m = 1$
3.572	40.5	44.6
3.8	33.4	38.8
4.093	25.5	33.8
4.5	15.2	30.4
4.71	10.2	30.3

TABLE 3. Values of R_c for a range of v in a straight-walled ($m = 0$) and curved-walled ($m = 1$) channel at $\sigma_1 = 0$

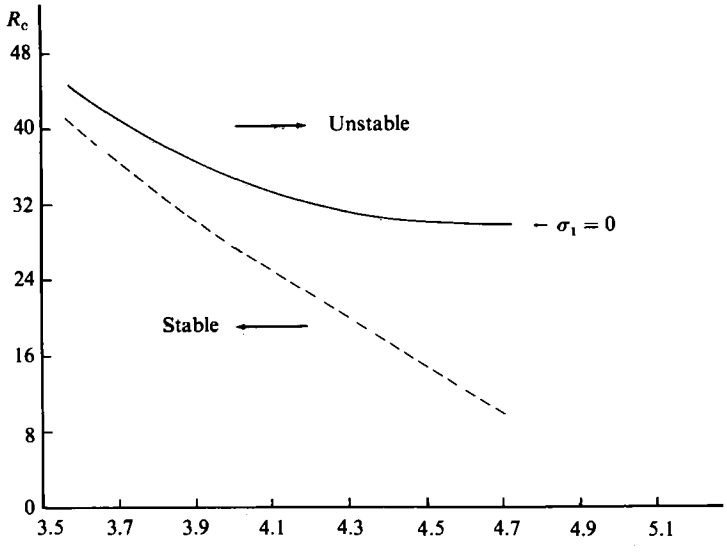

FIGURE 13. Boundary curve separating stable and unstable flow for the curved-walled channel ($m = 1$): ----, $m = 0$; ——, $m = 1$.

are computed for fixed v. A new β_c is interpolated corresponding to the minimum $\mathrm{GR}_\xi(\hat{E})$ (figure 12*a*). With this new β_c and three consecutive values of R (centred on R_c), the values of $\mathrm{GR}_\xi(\hat{E})$ are again computed. Another routine is used to interpolate or extrapolate an R corresponding to $\mathrm{GR}_\xi(\hat{E}) = 0$ (figure 12*b*). With this new set of (R_c, β_c) the process is repeated until convergence is achieved (Eagles & Smith 1980). The scheme is carried out for different values of v, and table 3 provides the results for the cases $m = 0$ and $m = 1$. These results are also illustrated in figure 13. To answer the first question partly, the results show that the case $m = 1$ is more stable than the case $m = 0$ at $\sigma_1 = 0$.

The interpolation/extrapolation procedure may be checked by establishing the necessary neutral curves and using these to determine R_c. This proved conclusive for all the values of v in table 3, and two particular neutral curves are illustrated in figures 14 and 15. To answer the first question completely we need to consider a range of m. For the case $m = -1$ we find that at $\sigma_1 = 0$ the flow appears to be more unstable than the case $m = 0$; this is consistent with the effect of curvature on the basic flow,

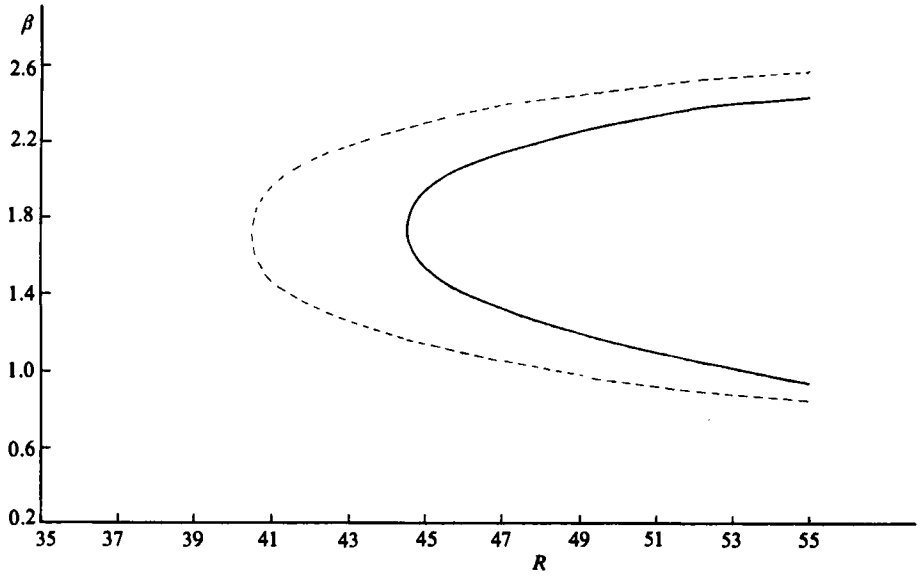

FIGURE 14. Neutral-stability curves for the curved walled channel ($m = 1$) at $\sigma_1 = 0$ with $v = 3.572$: ----, $m = 0$; ——, $m = 1$.

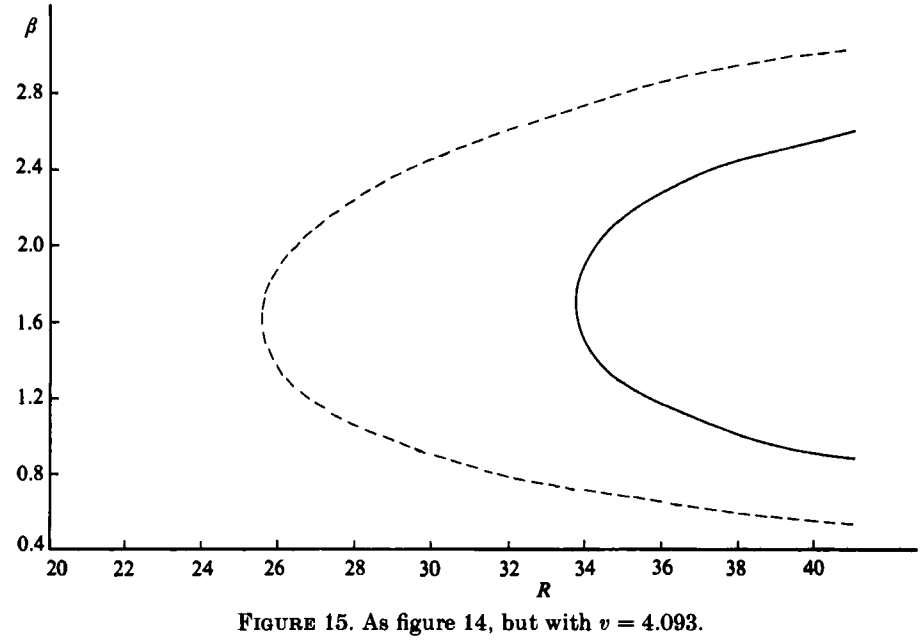

FIGURE 15. As figure 14, but with $v = 4.093$.

as illustrated in figure 4. Other values of R_c for a modest range of m demonstrate the general behaviour. A graph of R_c versus m for the case $v = 3.572$ is given in figure 16. This fairly linear relationship is useful in establishing R_c for a particular channel curvature (through m) and a particular class of Jeffery–Hamel profiles (through v).

The results in table 3 also answer the second question. The wedge cannot be used

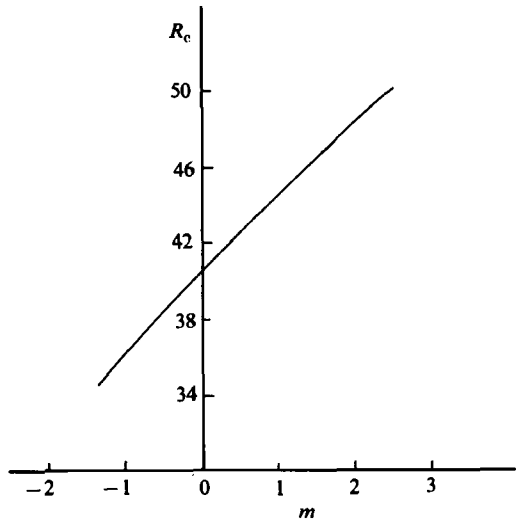

FIGURE 16. The relationship between R_c and the curvature parameter m at $\sigma_1 = 0$ and $v = 3.572$.

as a reasonable approximation to the curved-walled channel, since the final values of R_c ($m = 1$) are significantly distant from the initial values provided by the results of the straight-walled channel.

It is interesting to see what, if anything, predominantly accounts for the shifts in R_c given in table 3. We have already seen that in the case of $m = 0$ a smaller velocity along the centre of the channel (smaller v) is clearly associated with a more stable flow and hence a higher R_c. We may ask 'since the velocity profiles at $\sigma_1 = 0$ for the case $m = 1$ are smaller (along the centre of the channel) than the corresponding cases of $m = 0$ (figures 3*a* and 3*b*), does this fact account for most of the increase in R_c?' To answer this question, we may examine the effect on R_c, in the straight-walled channel, by substituting Ω based on $m = 1$ for a particular v, in place of Ω based on $m = 0$. This was done for cases available; and typically for the case $v = 3.572$ the shift in R_c went from 40.5 to 45.3. This is close to the result for $m = 1$ ($R_c = 44.6$). We conclude that the shift is strongly influenced by the change in the steady state associated with curvature, rather than higher-order terms or non-parallel effects.

8. A Fraenkel-type channel

This analysis is undertaken to study a more realistic channel. The channel is given by

$$\alpha(\tau) = \epsilon^{\frac{1}{2}} m_1 \operatorname{sech}^2 \tau. \tag{56}$$

We define σ ($= \epsilon\xi$) in terms of two new parameters σ_0 and σ_1:

$$\sigma = \sigma_0 + \epsilon^{\frac{1}{2}}\sigma_1, \tag{57}$$

where σ_0 is a constant and represents any fixed position in the channel. The new slow variable σ_1 is not the same as the previous σ_1, it is explicitly defined by (57) and $\partial/\partial\xi = \epsilon^{\frac{1}{2}}\partial/\partial\sigma_1$, as before.

This channel satisifies the condition required by Fraenkel (1963); that is, $\alpha(\tau) \to$ a

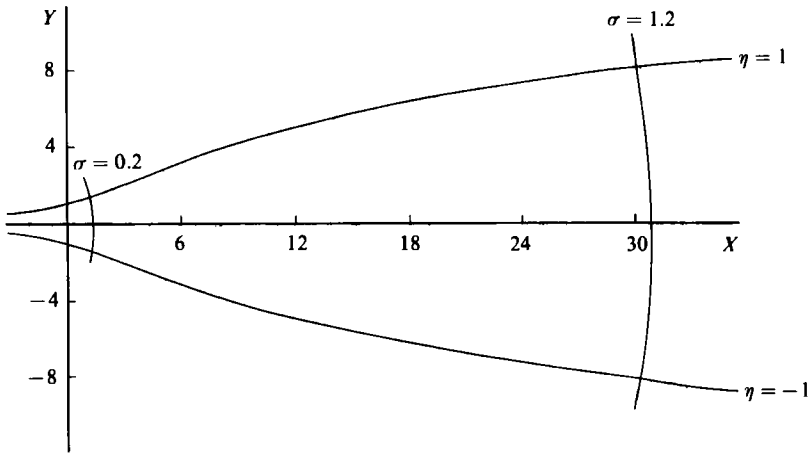

FIGURE 17. A Fraenkel-type channel given by $\alpha(\tau) = \epsilon^{\frac{1}{2}} m_1 \operatorname{sech}^2 \tau$ with $\epsilon^{\frac{1}{2}} = 0.4$ and $m_1 = 1$.

real constant as $\sigma \to \pm\infty$, and $\alpha(\tau)$ is real on $\eta = 0$. All the equations and results are taken up to and including the $O(\epsilon)$ term. The same notation is used as in the previous analysis, unless stated otherwise. Proceeding as before, we obtain

$$z = \frac{K_1}{\epsilon} \int_{\sigma_0}^{\tau} \exp\left[m_1 \tanh\left(\frac{s}{\epsilon^{\frac{1}{2}}}\right)\right] \mathrm{d}s + K_2. \tag{58}$$

The real constants K_1 and K_2 correspond to different z-scales and choice of origin. The integral is evaluated by adapting Simpson's rule along complex paths. Approximate analytical expressions can be found for (58) by reducing it to integrals of a complex function along real paths (Fraenkel 1963). These expressions illustrate an important difficulty associated with Fraenkel's coordinate system. The ratio of the final throat width to the initial throat width can become 'enormous' for particular cases of interest. However, it is possible to choose the parameters defining the channel so that, in the σ-range of interest, this ratio is not 'enormous'. A particular channel is illustrated in figure 17 with $\epsilon^{\frac{1}{2}} = 0.4$ and $m_1 = 1$. This channel is within experimental limits, and interesting features such as reverse flow near the walls is possible. Without loss of generality, we take $K_1 = 1$ and $K_2 = 0$.

The steady-state equations are derived in the same manner described in §4. New expressions can be found for κ and λ in powers of $\epsilon^{\frac{1}{2}}$. The resulting equations for Ω_0, Ω_1 and Ω_2 are very similar to the ones already given in Appendix (1 A). The only differences arise from the definition of $\alpha(\tau)$. In fact, expressions for the new equations may be deduced by referring to Appendix (1 A) and replacing $1 + m\sigma$ by $m_1 \operatorname{sech}^2 \sigma$. For a more general $\alpha(\tau)$, $v(1 + m\sigma)$ is replaced by $R\alpha(\sigma)$.

The new equations for G_0, G_1, G_2, F_0, F_1 and H_0 are given in Appendix (3 A). A comparison between these new equations and those in Appendix (1 B) reveals an interesting consistency. The parameter l originally defined in (12) plays an important role in this analysis. In fact, the parameters l and m may be used as transformation parameters. The choice of

$$l = m_1 \operatorname{sech}^2 \sigma_0, \quad m = -2m_1 \operatorname{sech}^2 \sigma_0 \tanh \sigma_0 \tag{59}$$

	$O(\epsilon^{\frac{1}{2}})$		$O(\epsilon)$				$O(\epsilon^{\frac{1}{2}})$		$O(\epsilon)$		
v	R_c	β_c	R_c	β_c	σ	v	R_c	β_c	R_c	β_c	σ
3.0	99.12	1.48	101.67	1.46	−0.4	4.5	35.94	1.81	38.15	1.74	−0.4
	71.24	1.64	73.85	1.60	−0.2		24.68	1.69	25.89	1.66	−0.2
	62.92	1.68	65.42	1.65	0.0		17.21	1.37	17.46	1.48	0.0
	69.50	1.65	71.97	1.62	0.2		15.91	1.23	14.77	1.44	0.2
	95.99	1.50	98.37	1.48	0.4		25.70	1.71	25.56	1.64	0.4
3.5	65.59	1.67	68.31	1.63	−0.4	4.7	33.12	1.80	35.16	1.74	−0.4
	46.93	1.78	49.31	1.72	−0.2		22.16	1.64	23.52	1.61	−0.2
	40.76	1.80	42.78	1.74	0.0		12.80	0.98	13.24	1.44	0.0
	44.32	1.79	46.32	1.73	0.2		20.33	1.54	18.58	1.49	0.4
	60.87	1.67	63.20	1.66	0.4		40.06	1.80	41.13	1.73	0.6
4.0	46.81	1.78	49.38	1.72	−0.4	4.8	32.01	1.79	33.95	1.73	−0.4
	33.06	1.79	34.88	1.73	−0.2		22.03	1.61	22.65	1.59	−0.2
	27.32	1.75	28.49	1.69	0.0		9.62	0.82	11.12	1.48	0.0
	28.58	1.76	29.83	1.70	0.2		17.30	1.34	13.63	1.41	0.4
	40.13	1.80	41.67	1.73	0.4		37.00	1.80	37.76	1.72	0.6

TABLE 4. R_c for a range of v, at various σ-planes including and excluding the $O(\epsilon)$ correction

transforms the previous system to this new system, with the exception of an additional term in the new equation for G_2. This term,

$$-2vm_1 \operatorname{sech}^2\sigma_0\,(3\tanh^2\sigma_0 - 1)\frac{\mathrm{d}G_0}{\mathrm{d}\eta}\frac{\mathrm{d}^2G_0}{\mathrm{d}\eta^2},$$

can be shown to result from the curvature varying more generally here. The addition of this term does not outweigh the important advantage of using (59), and hence utilizing the programs already coded in order to solve this new problem.

The term $h^2\,\partial(\mathrm{D}^2\Phi)/\partial t$ in (6) is bounded if Φ is defined by

$$\Phi(\xi,\eta,t) = \phi(\sigma_1,\eta;\sigma_0)\exp\left[\mathrm{i}(\theta(\xi)-\beta t')\right], \tag{60}$$

where

$$t' = \exp\left[-\frac{2m_1\tanh\sigma_0}{\epsilon^{\frac{1}{2}}}t\right] \tag{61}$$

and is the dimensionless time, scaled on the channel half-width at σ_0.

The equations for ϕ_0, ϕ_1 and ϕ_2 are given in Appendix (3 B). A comparison of these with the previous equations (30)–(32) show that the transformations in (59) are valid here also. The additional term in M_6, $-\mathrm{i}\beta_\mathrm{I} m_1[\frac{2}{3}\sigma_1^3(1+2\tanh^2\sigma_0)]\,(\mathrm{D}_1^2-k^2)$, arises from the extra term in G_2. The transformations are also valid for the growth rates, and they are implicitly contained in (54).

The general scheme for the stability analysis is to consider fixed values of v and establish the R_c value based on $\mathrm{GR}_\xi(\hat{E})$, at various σ stations, using the method already described in §7.

The shape of these channels gives us an insight into the behaviour of R_c. We expect a higher R_c far upstream and downstream, where the angle of divergence is closer to zero, than near a region where the angle of divergence reaches its maximum ($\sigma \approx 0$). Thus for each v we are able to interpolate an overall minimum R_c, R_c^*, corresponding to some β_c^* at some σ-station. These R_c are established for a range of v,

	$O(\epsilon^{\frac{1}{2}})$		$O(\epsilon)$		
v	R_c^*	β_c	R_c^*	β_c	σ
3.0	62.88	1.68	65.39	1.65	0.013
3.5	40.67	1.80	42.67	1.74	0.030
4.0	27.02	1.74	28.08	1.68	0.065
4.5	15.10	1.23	14.16	1.43	0.140
4.7	10.58	0.96	9.01	1.41	0.160
4.8	7.42	0.85	6.36	1.39	0.178

TABLE 5. The overall R_c, R_c^*, for a range of v, including and excluding the $O(\epsilon)$ correction

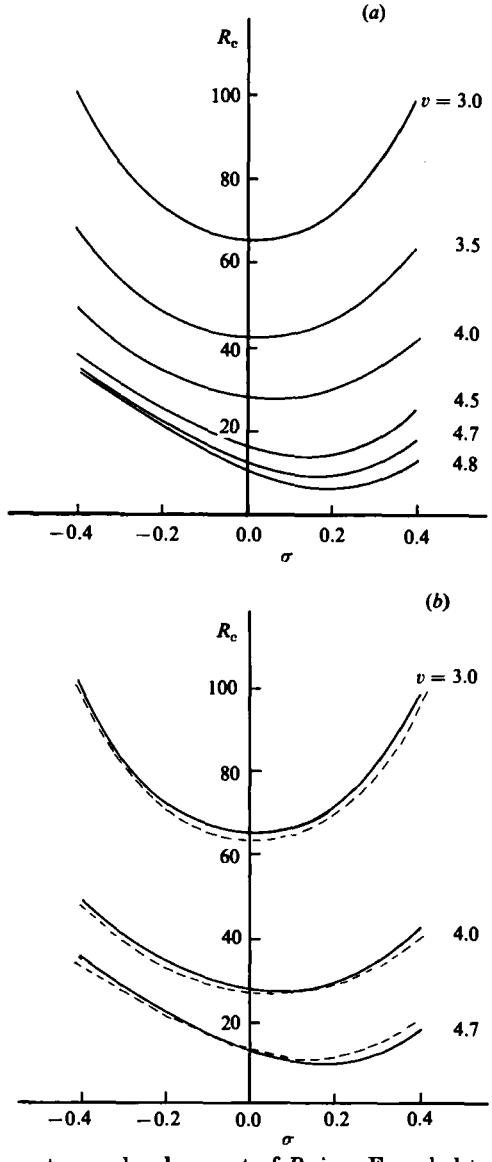

FIGURE 18. The downstream development of R_c in a Fraenkel-type channel ($m_1 = 1$), for different v-values at different orders: – – –, $O(\epsilon^{\frac{1}{2}})$; ——, $O(\epsilon)$.

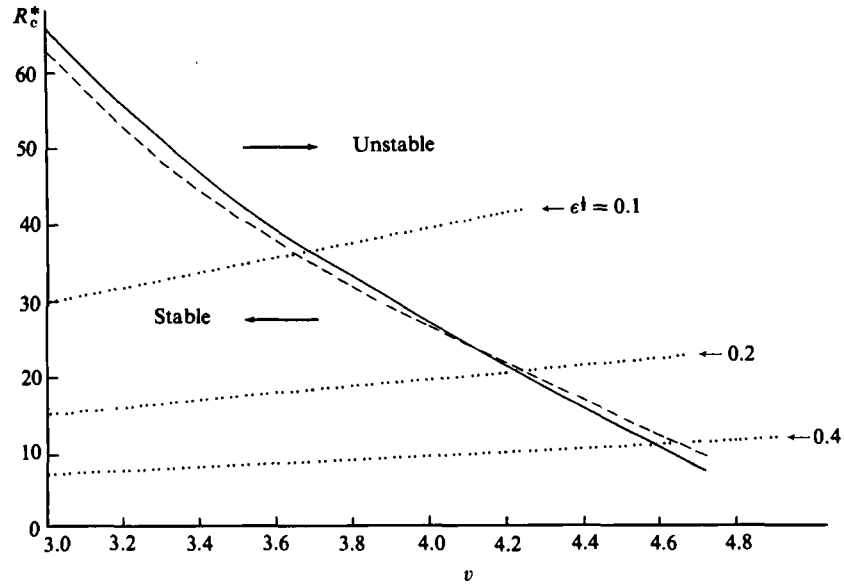

FIGURE 19. Boundary curves separating stable and unstable flow for a Fraenkel-type channel at different orders: ----, $O(\epsilon^{\frac{1}{2}})$; ——, $O(\epsilon)$.

including and excluding the $O(\epsilon)$ terms. This is necessary in order to justify the asymptotic development. The results are presented in table 4. The corresponding interpolated results for (R_c^*, β_c^*) are presented in table 5.

It is important to realize the problem associated with the steady-state flows characterized by $v \geqslant 4.7$. The class of Jeffery–Hamel profiles considered here are restricted to the simpler symmetric types with at most one region of reversed flow near each wall. This occurs when the values of v are not much bigger than 4.7. Eagles (1966) shows that, when we have regions of reversed flow, negative wave velocities are more likely to occur, and the neutral-stability curve goes below the R-axis, when R is plotted against β. It may not be possible to achieve critical points on the lower branch for positive values of β no matter how small β is chosen.

The results in table 4 are illustrated by figure 18(*a*), where R_c is plotted against σ for the $O(\epsilon)$ solution. The differences between the $O(\epsilon^{\frac{1}{2}})$ and the $O(\epsilon)$ solutions are shown in figure 18(*b*). These graphs show that to a small extent the $O(\epsilon)$ terms tend to stabilize the flow at all σ-stations for certain values of v. A v exists, however, in which the $O(\epsilon)$ term makes the flow more unstable. A similar result has already been discussed in §7.

A plot of R_c^* versus v is illustrated in figure 19. We recall the interpretation of such a curve (given in §7). Consider a fixed channel (define $\epsilon^{\frac{1}{2}}$ and m_1), and gradually increase R. A point (R, v) in figure 19 would then move along one of the dotted straight lines. In the case $\epsilon^{\frac{1}{2}} = 0.4$ and $m_1 = 1$ we see that when R just passes R_c^* (≈ 13) the growth of the disturbance characterized by $\mathrm{GR}_\xi(\hat{E})$ is just positive, and, by referring to table 5, we can estimate (using the $O(\epsilon)$ solution) that this occurs at $\sigma_1 \approx 0.15$ for a frequency $\beta \approx 1.42$. As R continues to increase, the disturbance grows for a range of σ and for a band of frequencies. These results are very similar in a qualitative way to the results of Eagles & Smith (1980), who effectively solved their problem up to $O(\epsilon^{\frac{3}{2}})$. Allmen's (1980) numerical solution of their problem, which could be considered a more accurate solution, exhibits the same feature as the $O(\epsilon)$ correction in this analysis.

9. Conclusion

If we consider the steady-state problem for the straight-walled channel, we find that the higher-order corrections are directly responsible for the increase in the steady-state velocity at the centre of the channel, and a decrease near the walls. This effect is small in general, but for larger values of v it can cause reverse flow near the walls (figure 2).

In the stability problem, the higher-order corrections do produce small shifts in the neutral-stability curves, even for relatively large values of $\epsilon^{\frac{1}{2}}$. A distinct stabilizing effect is present for values of v up to some v_c, and a destabilizing effect for values of v above v_c. This destabilizing effect for larger v is consistent with the reversed-flow effect (and hence more-unstable flow) described above.

The comparison of flows in curved-walled channels (curvature constant in sign) with divergent straight-walled channels at positions where the angle of divergence is the same ($\sigma_1 = 0$) shows that for $m > 0$ (divergent curved walls) the flow is more stable, while for $m < 0$ (convergent curved walls) the flow is more unstable. As we move further downstream ($\sigma_1 > 0$), we find perhaps the more natural results that for $m > 0$ the flow is more unstable, and for $m < 0$ the flow is more stable. The major contributor to these effects is shown to be the change in Ω associated with curvature, rather than general non-parallel and higher-order terms.

A Fraenkel-type channel, which might be constructed for experimentation, is shown to be more stable far upstream and downstream than near a region where the angle of divergence is a maximum ($\sigma = 0$) – the most-unstable region being downstream of $\sigma = 0$. The terms stable and unstable are used in a special sense in this investigation (§6), and it would be interesting to see how close the results presented here agree with those found in experiment.

This investigation was completed while one of the authors (G.A.G.) was a part-time student at The City University, London.

One of the authors (G.A.G.) would like to express his appreciation to Dr B. S. Massey (Department of Mechanical Engineering, University College London) for valuable discussions on fluid flow in channels.

REFERENCES

Allmen, M. 1980 Ph.D. thesis, Dept Mathematics, The City University, London.
Bouthier, M. 1972 *J. Méc.* **11**, 599.
Bouthier, M. 1973 *J. Méc.* **12**, 75.
Drazin, P. G. 1974 *Q. J. Mech. Appl. Maths* **27**, 69.
Eagles, P. M. 1966 *J. Fluid Mech.* **24**, 191.
Eagles, P. M. 1973 *J. Fluid Mech.* **24**, 149.
Eagles, P. M. & Weissman, M. A. 1975 *J. Fluid Mech.* **69**, 241.
Eagles, P. M. & Smith, F. T. 1980 *J. Engng Maths* **14**, 219.
Fraenkel, L. E. 1962 *Proc. R. Soc. Lond.* A **267**, 119.
Fraenkel, L. E. 1963 *Proc. R. Soc. Lond.* A **272**, 406.
Gaster, M. 1974 *J. Fluid Mech.* **66**, 465.
Georgiou, G. A. & Ellinas, C. P. 1985 *Intl J. Num. Meth. Fluid Dyn.* **5**, 169.
Goldstein, S. 1938 *Modern Developments in Fluid Dynamics.* Clarendon.

INCE, E. L. 1956 *Ordinary Differential Equations*. Dover.
LANCHON, H. & ECKHAUS, W. 1964 *J. Méc.* **3**, 445.
LIN, C. C. 1951 *Proc. Symp. Appl. Maths* **4**, 19.
LING, C. H. & REYNOLDS, W. C. 1973 *J. Fluid Mech.* **59**, 571.
ROSENHEAD, L. 1940 *Proc. R. Soc. Lond.* A **175**, 436.
SHEN, S. F. 1961 *J. Aero. Space Sci.* **28**, 397.
SMITH, F. T. 1979 *Proc. R. Soc. Lond.* A **336**, 91.
ZOLLARS, R. L. & KRANTZ, W. B. 1980 *J. Fluid Mech.* **96**, 585.